ACCIDENTAL FIRES AND RADIATION HEAT TRANSFER

Student Authors

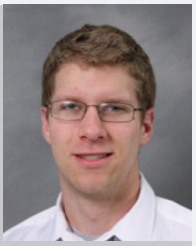

Nathaniel A. Bergman is a graduating senior in the School of Mechanical Engineering at Purdue University. Bergman is now employed by Siemens in the Infrastructure and Cities Sector and will be participating in Siemens' Engineering Leadership Development Program. At Purdue, Bergman was president of the Mechanical Engineering Honor Society Pi Tau Sigma, worked as an undergraduate research assistant in both the Summer Undergraduate Research Fellowship (SURF) and Discovery Park Undergraduate Research Internship (DURI) programs, interned at General Motors Powertrain in the Extended Range Electric Vehicles Division, and rowed on the Purdue Crew Team.

Subhrajit Chakraborty is a current senior in mechanical engineering at Purdue University. During his time at Purdue, Chakraborty was a teaching assistant and a tutor for the Physics Department. He also was a participant of the Global Engineering Alliance for Research and Education (GEARE) Germany (2013) program. In Germany, he attended a semester at the prestigious Karlsruhe Institute of Technology and interned with GEA Refrigeration Technologies where he worked on screw compressor technology. Chakraborty's research journey began as a participant in Purdue's SURF program during summer 2012. He plans to attend graduate school and follow his interest in thermal and fluid sciences.

Mentors

Brent A. Rankin is a research engineer for Innovative Scientific Solution Inc. at the Air Force Research Laboratory in Dayton, Ohio. He earned his BS, MS, and PhD from Purdue University's School of Mechanical Engineering. His research focused on developing new methods for quantitatively comparing images of the infrared radiation intensity from turbulent reacting flows.

Jay P. Gore is the Reilly University Chair Professor at the School of Mechanical Engineering with courtesy appointments in the School of Aeronautics and Astronautics and the School of Chemical Engineering at Purdue University. Gore has served as founding director of the Energy Center in Discovery Park, a Jefferson Science Fellow, and a founder of the SURF program.

Abstract

Accidental fires and their effects on the structural integrity of buildings are responsible for significant loss of human lives, economic assets, and environmental resources in the United States and across the globe. One cause of the collapse of the World Trade Center and the collapse of the Deepwater Horizon drilling platform in the Gulf of Mexico was the failure of structural materials under large heat loads from fires. Flame impingement or flame structure interaction studies are essential for understanding the effects of fire on the structural integrity of buildings. Radiation is an important mode of heat transfer to the structural element, and measurements of radiation intensities from the flame are useful for improving the understanding of heat transfer from the flame to the structure. This study investigates the radiation intensities and radiation heat flux from flames with and without impingement on a flat steel plate based on plate location relative to burner, fuel mass flow rate, and fuel type. The quantitative comparison between measured radiation intensities of impinging and non-impinging flames shows significant increases in radiation intensities near the surface of the plate. The radiation heat flux to the environment is lower for impinging flames, indicating high heat transfer to the plate. Quantitative knowledge gained from this study can be used to estimate structural integrity under large heat loads and to manufacture structural elements that are more resistant to fire.

Bergman, N. A. & Chakraborty, S. (2013). Accidental fires and radiation heat transfer: Investigating the effects of flame impingement on structures. *Journal of Purdue Undergraduate Research*, 3, 16–23. http://dx.doi.org/10.5703/jpur.03.1.03

Keywords

combustion, radiation, imaging, heat transfer, impingement, thermal sciences, impinging flame

http://dx.doi.org/10.5703/jpur.03.1.03

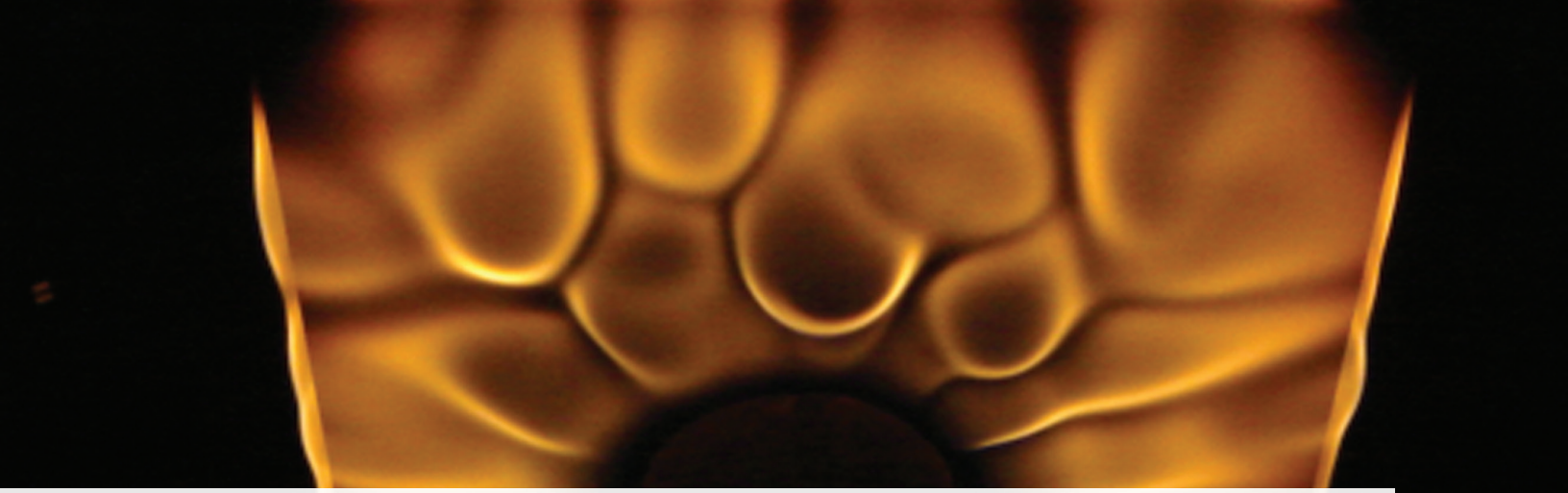

ACCIDENTAL FIRES AND RADIATION HEAT TRANSFER:

Investigating the Effects of Flame Impingement on Structures

Nathaniel A. Bergman and Subhrajit Chakraborty, Mechanical Engineering

INTRODUCTION

Fire is one of the most important discoveries in history and has allowed for advances in energy utilization, power and propulsion, and transportation applications. Conversely, unwanted and uncontrolled fires are responsible for significant losses. Strengthening the science and engineering basis for new standards and technologies is critical for reducing the nation's fire losses and managing national security interests. Fires engulfing structures are studied in this work using quantitative high-speed imaging of infrared radiation intensity, spectral radiation intensity measurements, and radiation heat flux measurements. Quantitative images, such as those reported in this work, are useful for estimating structure and fire temperatures, monitoring structure deflections, and comparing with fire simulation results (Rankin, Blunck, Katta, Stouffer, & Gore, 2012). Radiation intensity measurements provide benchmark fire data for prompting fire simulation improvements, suggesting new standards for structures under large heat loads, and developing new fire safety technologies.

Fire structure interactions have been explored in several past studies. Studies performed by You and Faeth (1979) focused on heat transfer to a ceiling from an impinging diffusion flame. Studies performed by Kokkala and Rinkinen (1987) defined time-dependent flame impingement patterns as a function of a number of characteristics such as fuel type and mass flow rate. This work was continued by Zhang and Bray (1999), who found flame shape to be dependent upon the nozzle exit velocity and distance between the nozzle and impingement structure for a given fuel type. Most recently, Newale, Rankin, and Gore (2012) studied the radiation intensity emitted from flames with and without impingement on a plate. These novel analytical methods have begun to computationally model the radiation intensity from non-impinging and impinging flames for quantitative comparison with experimental results. Motivated by these considerations, the objective of this work is to obtain quantitative knowledge about fire structure interactions under large heat loads.

Experiments are performed using a spectrometer, infrared (IR) camera, and radiometer to acquire quantitative radiation measurements of flames. The radiation intensity (I) measured by the IR camera is related to the solution of the radiative transfer equation shown in equation (i) (Modest, 2003). Equation (i) mathematically describes the I as a function of incident spectral intensity (I_λ), spectral absorptivity (α_λ), optical thickness (τ_λ), and blackbody spectral radiation intensity ($I_{b\lambda}$). α_λ accounts for the transmission losses through the filter and lens, as well as the response of the camera detector. τ_λ is the integral of the spectral absorption coefficient over the path length.

(i).

$$I = \int_{\lambda_1}^{\lambda_2} \alpha_\lambda I_\lambda(0) e^{-\tau_\lambda} \, d\lambda + \int_{\lambda_1}^{\lambda_2} \int_{0}^{\tau_\lambda} \alpha_\lambda I_{b\lambda}(\tau_\lambda^*) e^{-(\tau_\lambda - \tau_\lambda^*)} \, d\tau_\lambda^* \, d\lambda$$

The integrals are bounded over the range of wavelengths (λ_1 to λ_2), which represent the limits of the band-pass filter. Equation (i) shows that the radiation intensity is exponentially related to the temperature and concentration of gas species. Changes in temperature typically have a greater effect on the radiation intensity than those in concentrations.

The radiation heat loss fraction is defined as the ratio of energy released as radiation to total heat released due to combustion.

(ii).

$$X_r = \frac{\dot{Q}_r}{\dot{Q}} = \frac{\dot{Q}_r}{\dot{m} \cdot H_C}$$

In equation (ii), X_r is the radiation heat loss fraction, $\dot{Q}_r$ is the radiation heat loss to the surroundings, and $\dot{Q}$ is the heat release rate. $\dot{Q}$ is calculated as the mass flow rate of fuel $\dot{m}$ multiplied by the theoretical heat of combustion of the fuel H_C.

The current work investigates the interactions of buoyant diffusion flames with a structure by measuring the radiation intensity, spectral radiation intensity, and radiation heat flux using an infrared camera, spectrometer, and radiometer, respectively. The effects of the distance from the burner to the obstructing structure, the mass flow rate of fuel, and the type of fuel for both the impinging and non-impinging flames are studied.

EXPERIMENTAL METHODS

The turbulent buoyant diffusion flames are established using a diffuser burner with an exit diameter of 7.1 cm (Xin, Gore, McGrattan, Rehm, & Baum, 2005; Biswas, Zheng, Kim, & Gore, 2007). The burner is designed such that the gaseous fuel exits with an approximately uniform velocity (Xin et al., 2005). Turbulent buoyant diffusion flames are used to model accidental fires in a laboratory-scale environment. The mass flow rate of fuel is calibrated using a dry test turbine meter and controlled by setting the pressure upstream of a choked orifice plate. The total heat release rate of the flame is 4.2 kW under the assumption of complete combustion, and the visible flame height is approximately 36 cm (Xin et al., 2005). Measured and computed vertical and horizontal velocities and temperature values for this flame have been reported (Zhou et al., 1998; Xin et al., 2005).

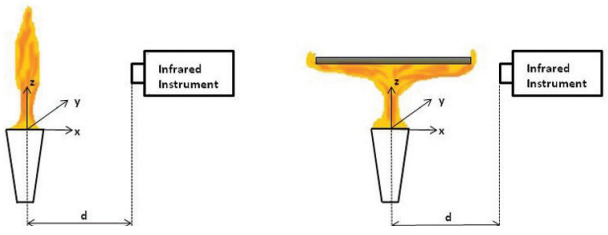

Figure 1. Experimental arrangement for radiation intensity measurements of the non-impinging (left) and impinging (right) buoyant diffusion flames acquired using an infrared camera and spectrometer.

A schematic of the experimental arrangement and coordinate system is illustrated in Figure 1. The coordinate system (x, y, z) is defined with an origin located at the center of the burner exit. For the impinging flame, a steel plate (22.8 cm by 22.8 cm by 1.3 cm) is suspended by a rod attached to the center of the plate. The plate is oriented such that the center of the plate coincides with the center of the flame, and the edges of the plate are parallel to the x- and y-axes. The plate is suspended at four axial locations (z/D = 0.25, 0.5, 1, 2) above the burner exit. The operating conditions include fuel type (methane or propane), mass flow rate (84.3 or 168.6 mg/s), and whether or not the flame impinges upon a steel plate. Measurements are taken during the initial stages of plate heating, thus ensuring the impingement plate remains near the ambient temperature (Weng & Hasemi, 2006).

The spectral radiation intensities (I_λ) from turbulent buoyant diffusion flames are acquired using a fast infrared array spectrometer (Zheng, Barlow, & Gore, 2003a; Zheng & Gore, 2005). I_λ is the radiation energy per unit time, per unit of projected area, per unit solid angle, and per unit wavelength (Bergman, Levine, Incropera, & Dewitt, 2011). The spectrometer detects radiation between 1.07–4.75 μm. The spectrometer is mounted perpendicular to the z-axis at a distance (d) of 30 cm from the burner center (in the x-direction), as shown in Figure 1. For the impinging flame, the plate is positioned outside of the small view angle of the spectrometer to minimize the effects of radiation from the plate on the measurements.

The IR camera is used to measure images of the radiation intensity from the flames (Rankin, 2012; Rankin et al., 2012; Rankin, Blunck, & Gore, 2012). Band-pass filters are positioned between the camera lens and detector to isolate the radiation emitted by specific combustion products such as carbon dioxide (CO_2), water vapor (H_2O), and soot. The band-pass filters used in this work allow radiation with wavelengths of 2.58 ± 0.03 μm (H_2O) and 4.34 ± 0.10 μm (CO_2) to reach the detector. The spatial resolution of the measurements is approximately 0.9 mm.

The experimental uncertainty of the infrared camera measurements has been evaluated previously and is less than 15% with 95% confidence (Rankin, Blunck, & Gore, 2012). The IR camera and spectrometer are calibrated using a blackbody radiation source, and atmospheric absorption of the flame radiation is accounted for during this process.

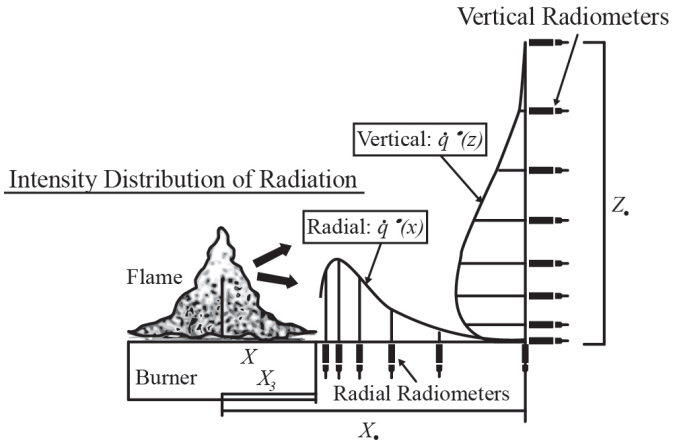

Figure 2. Schematic of the experimental arrangement used to measure the radiation heat flux distribution over a cylindrical surface surrounding the flame (Hamins, Kashiwagi, and Buch, 1995).

Figure 2 shows the experimental arrangement used to measure the radiation heat flux with a radiometer. The radiometer is moved radially away from the burner measuring the radiation heat flux denoted by *q"(x)* in Figure 2. Once X_0 is reached, the axis of the radiometer is rotated 90°. The radiometer is then moved in the axial direction measuring the radiation heat flux denoted by *q"(z)* until the radiation heat flux decreases to near zero at Z_0.

The procedure of collecting radiation heat flux measurements for the impinging flame is similar to the non-impinging flame. The plate is cooled at regular intervals to avoid heat flux from the plate being detected by the radiometer.

The total radiation heat loss from the flame is calculated by integrating the radiation heat flux measurements over the surface of an imaginary cylinder surrounding the flame (assuming axisymmetric) using the following equation:

$$\dot{Q}_r = 2\pi \int_0^{X_0} x \cdot q''(x) \cdot dx + 2\pi \cdot X_0 \int_0^{Z_0} q''(z) \cdot dz$$

The first integral consisting of the *q"(x)* term integrates the radiation heat flux over the area of the base of the imaginary cylinder. The second integral consisting of the *q"(z)* term integrates the radiation heat flux through the lateral surface of the imaginary cylinder. It is assumed that the radiation heat flux through the upper surface of the cylinder is negligible, because the radiometer is moved axially upward to a location where no significant radiation

Figure 3. Qualitative images of visible radiation emitted by the propane (C_3H_8) impinging flame for a range of plate positions and fuel mass flow rates.

is measured. After calculating the total radiation heat loss using equation (iii), the radiation heat loss fraction is calculated using equation (ii).

RESULTS AND DISCUSSION

Qualitative Images of Visible Radiation Intensity

Figure 3 shows qualitative images of the radiation emitted in the visible spectrum from the propane flames impinging on the steel plate for a range of plate positions above the burner (z/D = 0.25, 0.50, 1.00, and 2.00) and two fuel mass flow rates (84.3 and 168.6 mg/s). The visible images depict a region of high-intensity flames near the edges of the impingement plate, especially at high mass flow rates. A cellular or bubble pattern is observed for the impinging flame with a mass flow rate of 168.6 mg/s and plate positioned at z/D = 0.25 above the burner. Broken concentric rings are apparent in the visible images of the impinging flames for both mass flow rates and the plate positions of z/D = 1.00 and 2.00. This ring pattern is caused by periodic pulsations of the flame.

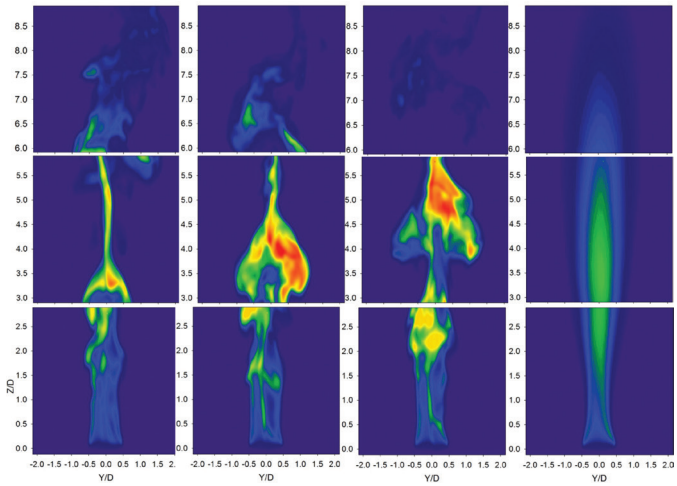

Figure 4. Quantitative time-dependent and time-averaged images of the infrared radiation intensity emitted by CO_2 (4.34 ± 0.10 μm) for the non-impinging methane flame with a mass flow rate of 168.6 mg/s.

Quantitative Images of Infrared Radiation Intensity

Figure 4 illustrates representative quantitative images of the radiation intensity from the non-impinging buoyant diffusion flame acquired using the infrared camera. The instantaneous images (first three columns) are temporally related from left to right, with approximately 0.058 seconds between each image. The instantaneous images are spatially related from top to bottom. The effects of turbulence on the flame are evident as observed by the fluctuation in flame size and intensity as a function of time and space.

The last column in Figure 4 shows the quantitative time-averaged image of the infrared radiation intensity from the non-impinging turbulent buoyant diffusion flame. It is important to note that when an average image is obtained, there is a significant drop in the maximum intensity exhibited by the flame. This is caused by the turbulent fluctuations in the flame which results in instants with radiation intensity values above and below the mean intensity.

Time-averaged images have been acquired for two fuels (CH_4 and C_3H_8), one mass flow rate (84.3 mg/s), and two radiating gas species (CO_2 emitting near 4.34 ± 10 μm and H_2O emitting near 2.58 ± 0.03 μm). The radiation intensities along the image centerlines are shown in Figure 5.

The radiation intensity emitted by H_2O vapor when propane is the fuel is about two times that emitted when methane is used. The mole fraction of water vapor when methane (0.180) is burned is greater than that for propane (0.148) when complete combustion occurs. When adiabatic flame temperatures are compared (obtained using chemical equilibrium calculations), it is clear that propane (2267K) results in higher temperatures than

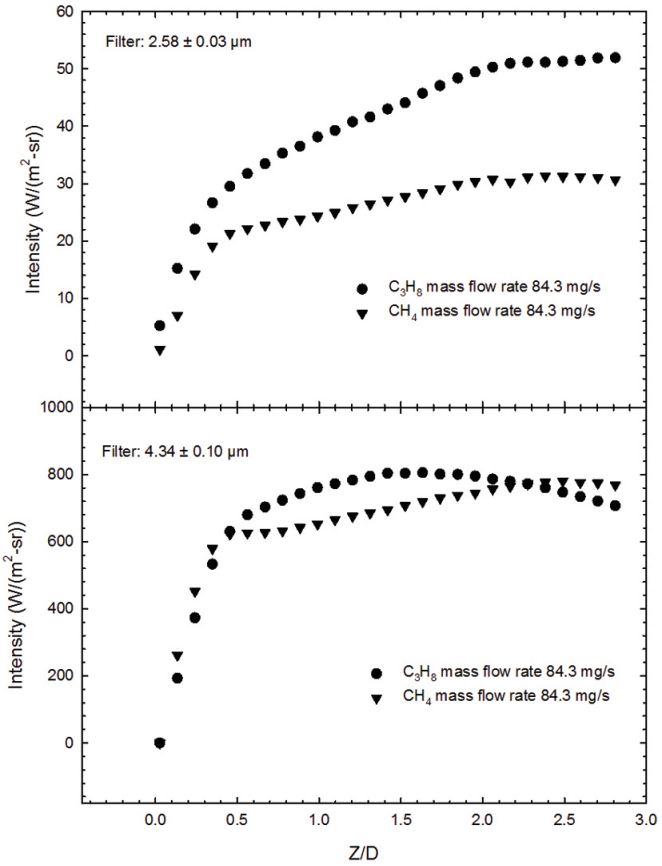

Figure 5. Radiation intensities along non-impinging flame centerline emitted by H_2O vapor (top) and CO_2 (bottom) as a function of distance above the burner exit.

methane (2226K). Temperature plays a greater role in radiation intensity than concentration. The difference in the adiabatic flame temperatures for methane and propane is one reason for the higher radiation intensity emitted by water vapor observed for the propane flame.

The radiation intensity emitted by CO_2 is greater for propane over most of the flame. The concentration of CO_2 when propane is burned is greater than that when methane is the fuel. Therefore, propane flames should have greater radiation intensity than methane flames, as observed in Figure 5.

One of the differences between the impinging and non-impinging flames is the increase in radiation intensity near the bottom surface of the impingement plate. The time-averaged intensity for the impinging flame is approximately two times larger than the intensity measured for the non-impinging flame with the same fuel type and mass flow rate. Relative to the width of the non-impinging flame, the width of the impinging flame is greater. Greater flame width means larger path lengths. Larger path lengths for the impinging flames result in greater observed radiation intensities than those observed for the non-impinging flame.

An understanding of the spatial distribution of the radiation intensity around the plate is achieved by analyzing the quantitative infrared images. The location of the maximum intensity near the bottom surface of the impingement plate is affected by the distance between burner and the plate. When the plate and burner are close (z/D = 0.25 and 0.50), the maximum intensity is located near the edges of the impingement plate. The location of maximum intensity shifts toward the center of the flame when the burner is moved further away from the plate.

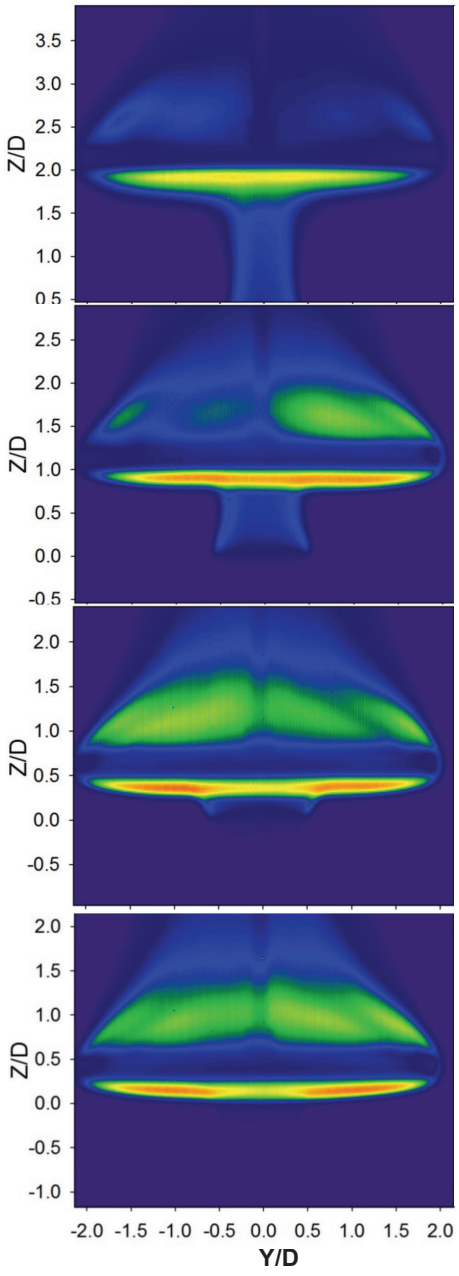

Figure 6. Time-averaged images of the infrared radiation intensity emitted by CO_2 (4.34 ± 0.10 μm) for the impinging methane flames with a mass flow rate of 168.6 mg/s for a range of plate positions (z/D = 0.25, 0.5, 1, and 2).

The impinging flames have lower intensities than the non-impinging flames in portions of the flame below the impingement plate. This effect is most noticeable at plate locations of z/D = 1.00 and 2.00. This lower intensity is caused by the formation of an envelope flame with a cool central core (Zhang & Bray, 1999). The envelope flame is characterized as a laminar flow, with a very well-defined flame sheet (Zhang & Bray, 1999; Turns, 2000). The cool central core results in limited combustion at the flame's axis. Limited combustion results in lower temperatures and concentrations of combustion products, ultimately yielding lower radiation intensities when compared with the non-impinging flame.

Spectral Radiation Intensity Measurements

Figure 7 compares the I_λ measurements of the non-impinging and impinging flames. The impingement plate acts as an obstruction and increases the concentration of carbon dioxide and other combustion products near the bottom surface of the plate. There is an increase in the flame width near the bottom surface of the plate. The increase in the concentration of radiating combustion products and increase in flame depth causes the radiation for the impinging flame to be larger than that from the non-impinging flame in agreement with the IR camera

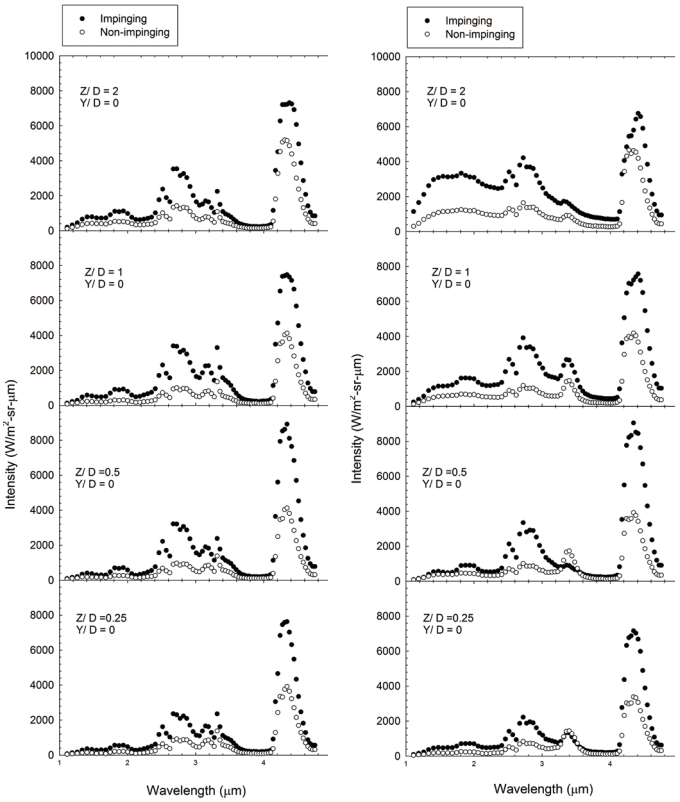

Figure 7. Spectral radiation intensities from diametric path for impinging and non-impinging methane flames (left) and propane flames (right) with a mass flow rate of 84.3 mg/s.

measurements. Soot radiates as a black body over all wavelengths. It is observed that the radiation from soot increases with increasing distance from the burner (till z/D = 2) for both the non-impinging and impinging flames. This observation indicates the presence of larger soot volume fractions and soot temperatures.

There is a more significant contribution from soot to the spectral radiation intensity from propane flames in comparison to the methane flames. This is because of the higher carbon to hydrogen ratio in propane (3:8) in comparison to methane (1:4). The fuel with the higher carbon to hydrogen ratio produces more soot (carbon). According to prior work, the spectral radiation intensity from propane contains a peak centered at 3.37 µm (Wakatsuki, 2005). The peak observed between 3 µm and 3.5 µm in the spectral radiation intensity from the propane flames results from radiation emitted by the unburnt propane gas. The peak decreases with increasing distance from the burner, indicating less unburnt propane is present. This is due to the fact that the mixture of gases becomes more fuel lean while moving away from the burner, thus, the concentration of unburnt propane decreases.

The maximum spectral radiation intensity is emitted from CO_2 and occurs at wavelengths from approximately 4.2 to 4.6 µm as shown in Figure 7. The maximum spectral radiation intensities observed in the non-impinging flames typically increase with increasing height above the burner for both the methane and propane flames. For impinging flames, regardless of the fuel type, the maximum spectral radiation intensities are observed at 0.5 D away from the burner, for mass flow rate of 84.3 mg/s.

Radiation Heat Flux Measurements

The radiation heat loss fraction is approximately 10% for the non-impinging methane flame with a mass flow rate of 84.3 mg/s. This indicates that 10% of the energy released during combustion is radiated to the surroundings. The radiation heat loss fraction is approximately 6% for the impinging methane flame with a mass flow rate of 84.3 mg/s. The imaginary cylinder used for calculating the radiation heat loss fraction includes the flat plate. A significant part of the heat is transferred to the plate, which decreases the total energy radiated to the surroundings of the plate and the flame.

Figure 8 shows the radiation heat flux as a function of the radial distance from the flame centerline along the bottom surface of the imaginary cylinder. The radiation heat fluxes are similar for the non-impinging and impinging flames. This indicates that the radiation heat flux leaving the bottom surface of the imaginary cylinder is not affected by the introduction of a plate.

Figure 9 shows that the radiation heat flux values for the impinging flame decrease steeply after 15 cm, whereas the values for the non-impinging flame gradually decrease to zero. The sharp decrease is caused by the plate positioned at 14.2 cm above the burner. The cold plate blocks the radiation from the flame when the radiometer is positioned axially above the plate. The peak radiation heat flux for the impinging flame is higher than the non-impinging flame. The steel plate increases the concentration of combustion product gases such as carbon dioxide and water vapor, leading to an increase in emitted radiation near the bottom surface of the plate.

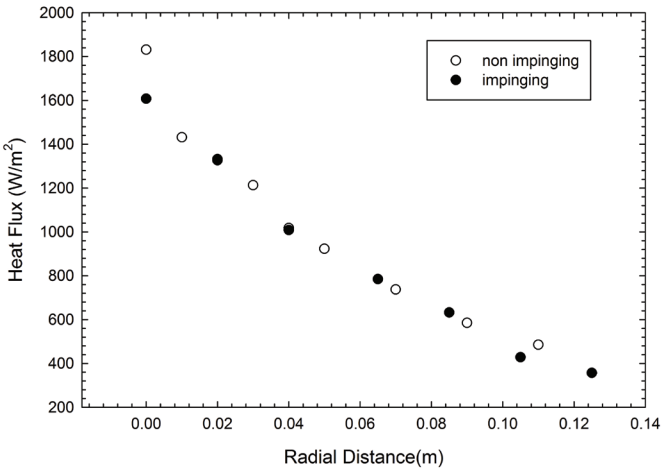

Figure 8. Radiation heat flux values in the radial direction for impinging and non-impinging methane flames (84.3 mg/s).

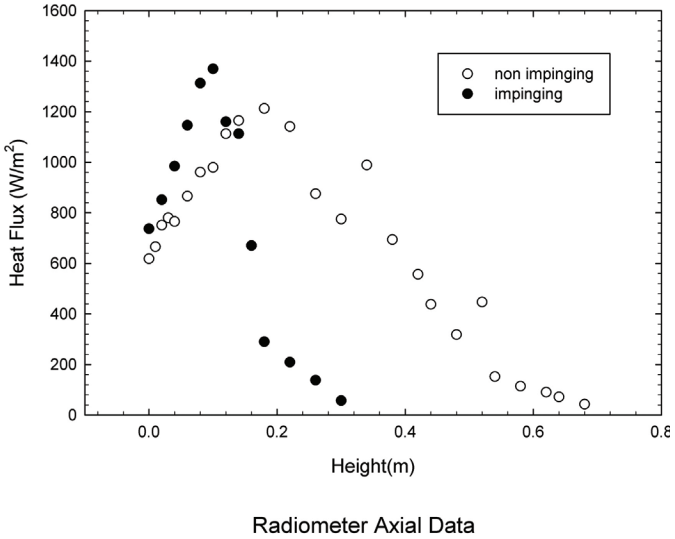

Figure 9. Radiation heat flux values in the axial direction for impinging and non-impinging methane flames (84.3 mg/s).

SUMMARY AND CONCLUSIONS

The IR camera and spectrometer measurements indicate that there is an increase in the radiation intensity near the impingement plate relative to the non-impinging flame. This increase in intensity is caused by the spreading of the flame, increase in radiating gas species concentration under the plate, and increase in temperature of the gas species. Higher gas species temperatures are representative of a hotter flame at the surface of impingement. Higher temperature flames increase the severity of accidental fires, increase fire spread rates, and ultimately cause greater potential for loss of life and property.

In addition to showing an increase in radiation intensity below the plate, the IR camera images display the spatial distribution of radiation intensity. For configurations where the burner is closer to the plate, the location of maximum intensity is near the edges of the plate. As the distance between the burner and plate is increased, the maximum intensity shifts toward the center of the flame. Also, at larger burner to plate distances, a steady envelope flame is visible, characterized by minimal combustion.

The spectral distribution of the radiation intensities shows the contribution from unburnt fuel to the overall radiation. It is observed that maximum radiation intensity is emitted by CO_2. Because of the greater radiation intensity emitted by CO_2 relative to other gases, higher concentrations of CO_2 under the structure will result in higher heat loads. Higher heat loads will lead to rapid failure of structural integrity. Additionally, fuels that have a greater carbon to hydrogen ratio result in increased production of soot and higher overall radiation emitted, thus creating a greater risk of structural failure.

The radiation heat flux measurements indicate that the steel plate absorbs approximately half of the radiative energy as compared to a non-impinging flame with similar operating conditions. This demonstrates the importance of designing heat-resistant structures that can withstand high heat loads from fires without failing.

ACKNOWLEDGMENTS

Thank you to the Summer Undergraduate Research Fellowship (SURF) program at Purdue University for providing funding and support of both authors' work. A special thanks is extended to Dr. Brent Rankin and Professor Jay Gore for their mentorship and guidance during the research and writing stages. Additionally, thank you to graduate students Robert Kapaku and Ashish Newale for aiding in analysis and writing. Finally, thank you to Elizabeth Hudson for her help in revising and editing this paper for publication.

REFERENCES

Bergman, T. L., Levine, A. S., Incropera, F. P., & Dewitt, D. P. (2011). *Fundamentals of heat and mass transfer* (7th ed.). Hoboken, NJ: John Wiley & Sons, Inc.

Biswas, K., Zheng, Y., Kim, C. H., and Gore, J. (2007). Stochastic time series analysis of pulsating buoyant pool fires. *Proceedings of the Combustion Institute, 31*(2), 2581–2588. http://dx.doi.org/10.1016/j.proci.2006.07.234

Hamins, A., Kashiwagi, T., & Buch, R. R. (1995, June). Characteristics of pool fire burning. *Proceedings of American Society of Testing and Materials, 1284*, 12–15.

Kokkala, M., & Rinkinen, W. J. (1987). Some observations on the shape of impinging diffusion flames. *Technical Research Centre of Finland, Research Reports,* 461–480.

Modest, M. (2003). *Radiative heat transfer.* San Diego: Academic Press.

Newale, A. S., Rankin, B. A., & Gore, J. P. (2012, April). *Radiation intensity measurements and computations of an impinging turbulent buoyant diffusion flame.* Paper presented at the Spring Technical Meeting of the Central States Section of the Combustion Institute, Dayton, Ohio.

Rankin, B. A., Blunck, D. L., & Gore, J. P. (2012). Infrared imaging and spatiotemporal radiation properties of a turbulent nonpremixed jet flame and plume. *Journal of Heat Transfer*, 135(2), 021201. http://dx.doi.org/10.1115/1.4007609

Rankin, B. A., Blunck, D. L., Katta, V. R., Stouffer, S. D., & Gore, J. P. (2012). Experimental and computational infrared imaging of bluff body stabilized laminar diffusion flames. *Combustion and Flame*, *159*(9), 2841–2843. http://dx.doi.org/10.1016/j.combustflame.2012.03.022

Rankin, B. A. (2012). Quantitative experimental and model-based imaging of infrared radiation intensity from turbulent reacting flows. (Doctoral dissertation). Purdue University, West Lafayette, Indiana. Retrieved from http://docs.lib.purdue.edu/dissertations/AAI3556575/

Turns, S. R. (2000). *An introduction to combustion: Concepts and applications* (2nd ed.). Boston: WCB/McGraw-Hill.

Wakatsuki, K. (2005). High temperature radiation absorption of fuel molecules and an evaluation of its influence on pool fire modeling. (Doctoral dissertation). University of Maryland, College Park, Maryland. Retrieved from http://hdl.handle.net/1903/2366

Weng, W. G., & Hasemi, Y. (2006). Heat transfer to an unconfined ceiling from an impinging buoyant diffusion flame. *Heat and Mass Transfer,* 42(7), 652–659. http://dx.doi.org/10.1007/s00231-005-0043-0

You, H. Z., & Faeth, G. M. (1979). An investigation of fire impinging on a horizontal ceiling. *U.S. Department of Commerce National Bureau of Standards Center for Fire Research.*

Xin, Y., Gore, J. P., McGrattan, K. B., Rehm, R. G., & Baum, H. R. (2005). Fire dynamics simulation of a turbulent buoyant flame using a mixture-fraction-based combustion model. *Combustion and Flame,* 141(4), 329–335. http://dx.doi.org/10.1016/j.combustflame.2004.07.001

Zhang, Y., & Bray, K. N. C. (1999). Characterization of impinging jet flames. *Combustion and Flame,* 116(4), 671–674. http://dx.doi.org/10.1016/S0010-2180(98)00084-4

Zheng, Y., Barlow, R. S., & Gore, J. P. (2003a). Measurements and calculations of spectral radiation intensities for turbulent non-premixed and partially premixed flames. *Journal of Heat Transfer, 125*(4), 678–686. http://dx.doi.org/10.1115/1.1589502

Zheng, Y., Barlow, R. S., & Gore, J. P. (2003b). Spectral radiation properties of partially premixed turbulent flames. *Journal of Heat Transfer, 125*(6), 1065–1073. http://dx.doi.org/10.1115/1.1621902

Zheng, Y., & Gore, J. P. (2005, January). Measurements and inverse calculations of spectral radiation intensities of a turbulent ethylene/air jet flame. *Proceedings of the Combustion Institute,* 30(1), 727–734. http://dx.doi.org/10.1016/j.proci.2004.08.255

Zhou, X. C., & Gore, J. P. (1998, August). Experimental estimation of thermal expansion and vorticity distribution in a buoyant diffusion flame. *Proceedings of the Combustion Institute,* 2, 2767–2773. Retrieved from http://fire.nist.gov/bfrlpubs/fire98/PDF/f98195.pdf